TRANSIENT FLUID FLOW IN HETEROGENEOUS POROUS MEDIA

by

Xiaomin Zhao and M. Nafi Toksöz

Earth Resources Laboratory
Department of Earth, Atmospheric, and Planetary Sciences
Massachusetts Institute of Technology
Cambridge, MA 02139

ABSTRACT

A stable Alternating Direction Implicit finite-difference algorithm is used to model transient fluid flow in heterogeneous porous media. In connection with the laboratory system for pressure transient testing of core permeability, the effects of permeability heterogeneities on the characteristics of the pressure transient were investigated. The results show that the early portion of the pressure transient is sensitive to the heterogeneity, while the late time portion is primarily controlled by the effective permeability of the sample. As in the steady flow case, lineation in permeability distribution produces anisotropy in measured permeability. Particularly, in the case of lineated fractures, where the background permeability is small, such anisotropy can produce an order of magnitude difference in permeability.

INTRODUCTION

Time-dependent fluid flow in permeable porous media is important both in the laboratory and field. In the field, the decay of pressure pulse with time in boreholes is used to measure permeability or fluid transport properties of the formation (Melville et al., 1991). While in the laboratory, pressure transients are commonly used to determine the permeability of low permeable samples (Brace et al., 1968; Kamath et al., 1990; Bernabé, 1991). In both situations, a commonly encountered problem is the effects of heterogeneous porous media on the transient flow characteristics. In the field, heterogeneities of different scales exist in the reservoir formations, an example of which is the sand-shale sequence. In reservoir rocks, flow network consists of fractures of different sizes. In these cases, the scale size of the heterogeneities relative to the penetration of the transient flow may control the flow field. Down to the laboratory scale of a few inches, the effect of heterogeneities still plays an important role in affecting the behavior of pressure transients. Kamath et al. (1990) showed that, due to the presence of sample

heterogeneities, the effective permeability calculated from the pressure transient test could change with the direction of pressure disturbance, and could differ significantly from the effective steady values. Given these facts, it is desirable to carry out a numerical study to investigate the effects of scale size and the distribution of a heterogeneous porous medium on the transient fluid flow.

The most effective numerical technique for simulating a heterogeneous medium is the finite difference method. Using the finite difference technique, Zhao and Toksöz (1991) have studied the effects of heterogeneity on the steady fluid flow in porous media. In this study, we apply a stable finite difference algorithm to model transient flow in an arbitrarily heterogeneous porous medium. We will model the effects of various heterogeneous distributions on the transient flow. As an application, we apply the finite difference code to model the transient flow for the experimental set-up constructed for measuring the permeability of laboratory core samples.

THEORY

In a two-dimensional (2-D) heterogeneous porous medium, the equation that describes the time-dependent fluid flow is given by

$$\frac{\partial}{\partial x}\left[\alpha\frac{\partial P}{\partial x}\right]+\frac{\partial}{\partial y}\left[\alpha\frac{\partial P}{\partial y}\right]=\frac{\partial P}{\partial t} \tag{1}$$

with

$$\alpha(x,y)=\frac{k(x,y)\kappa_f}{\mu\phi} \tag{2}$$

where μ is fluid viscosity, ϕ is porosity, κ_f is fluid incompressibility, and $k(x,y)$ is heterogeneous permeability as a function of the spatial coordinates x and y. Because α varies over the 2-D medium, numerical algorithms are required to solve the equation in connection with appropriate boundary conditions.

A STABLE FINITE DIFFERENCE IMPLEMENTATION USING THE ADI TECHNIQUE

A conventional technique for studying Eq. (1) is using the forward time-central space finite difference method. It can be shown that the stability of the method is given by $\alpha\frac{\Delta t}{\Delta x\Delta y}\leq\frac{1}{2}$ (Ferziger, 1981). This means that the time step Δt is restricted by the grid spacing Δx, Δy, and the value of α. In the case of a heterogeneous $\alpha(x,y)$, where $\alpha(x,y)$ can be very small (or large), this stability condition may be violated. In this study, we solve Eq. (1) using the Alternating Direction Implicit (ADI) method. This

is a powerful and stable algorithm for solving equations like Eq. (1) in a rectangular domain. Using the ADI algorithm, we rewrite Eq. (1) as

$$P_t = A_1 P + A_2 P \tag{3}$$

where $P_t = \frac{\partial P}{\partial t}$, $A_1 = \frac{\partial}{\partial x}\left(\alpha(x,y)\frac{\partial P}{\partial x}\right)$, and $A_2 = \frac{\partial}{\partial y}\left(\alpha(x,y)\frac{\partial P}{\partial y}\right)$. We discretize Eq. (3) using the Crank-Nicolson scheme, which is the center difference scheme about time $t = (n+1/2)\Delta t$. By using the Taylor expansion and taking the first order approximation, Eq. (3) becomes

$$\frac{P^{n+1} - P^n}{\Delta t} = \frac{1}{2}(A_1 P^{n+1} + A_1 P^n) + \frac{1}{2}(A_2 P^{n+1} + A_2 P^n) \ . \tag{4}$$

Eq.(4) can further be written as

$$\left(I - \frac{\Delta t}{2}A_{1h}\right)\left(I - \frac{\Delta t}{2}A_{2h}\right)P^{n+1} = \left(I + \frac{\Delta t}{2}A_{1h}\right)\left(I + \frac{\Delta t}{2}A_{2h}\right)P^n \ , \tag{5}$$

where A_{1h} and A_{2h} represent the following operators:

$$\begin{aligned} A_{1h}P &= \frac{1}{\Delta x^2}\left[B_{i+1,j}(P_{i+1,j} - P_{i,j}) - B_{i,j}(P_{i,j} - P_{i-1,j})\right] \\ A_{2h}P &= \frac{1}{\Delta y^2}\left[C_{i,j+1}(P_{i,j+1} - P_{i,j}) - C_{i,j}(P_{i,j} - P_{i,j-1})\right] \end{aligned} \tag{6}$$

with

$$\begin{aligned} B_{i,j} &= \frac{\alpha(i,j) + \alpha(i+1,j)}{2} \\ C_{i,j} &= \frac{\alpha(i,j) + \alpha(i,j+1)}{2} \ , \end{aligned}$$

and $i = 0, 1, 2, \cdots, I$, $j = 0, 1, 2, \cdots, J$.

Eq. (5) can be solved using the Peaceman-Rachford algorithm (Ferziger, 1981). This algorithm consists of splitting Eq. (5) into two separate equations by using an intermediate function $\tilde{P}^{n+1/2}$:

$$\left(I - \frac{\Delta t}{2}A_{1h}\right)\tilde{P}^{n+1/2} = \left(I + \frac{\Delta t}{2}A_{2h}\right)P^n \tag{7}$$

$$\left(I - \frac{\Delta t}{2}A_{2h}\right)P^{n+1} = \left(I + \frac{\Delta t}{2}A_{1h}\right)\tilde{P}^{n+1/2} \ . \tag{8}$$

Substituting Eqs. (6) into (7) and (8) results in

$$\begin{aligned} &-\frac{\Delta t}{2\Delta x^2}B_{i,j}\tilde{P}^{n+1/2}_{i-1,j} + \left[1 + \frac{\Delta t}{2\Delta x^2}(B_{i,j} + B_{i+1,j})\right]\tilde{P}^{n+1/2}_{i,j} - \frac{\Delta t}{2\Delta x^2}B_{i+1,j}\tilde{P}^{n+1/2}_{i+1,j} \\ &\quad = \frac{\Delta t}{2\Delta y^2}C_{i,j-1}P^n_{i,j-1} + \left[1 - \frac{\Delta t}{2\Delta y^2}(C_{i,j} + C_{i,j+1})\right]P^n_{i,j} + \frac{\Delta t}{2\Delta y^2}C_{i,j+1}P^n_{i,j+1} \end{aligned} \tag{9}$$

$$-\frac{\Delta t}{2\Delta y^2}C_{i,j}P_{i-1,j}^{n+1}+\left[1+\frac{\Delta t}{2\Delta y^2}(C_{i,j}+C_{i,j+1})\right]P_{i,j}^{n+1}-\frac{\Delta t}{2\Delta y^2}C_{i,j+1}P_{i,j+1}^{n+1}$$
$$=\frac{\Delta t}{2\Delta x^2}B_{i-1,j}\tilde{P}_{i-1,j}^{n+1/2}+\left[1-\frac{\Delta t}{2\Delta x^2}(B_{i,j}+B_{i+1,j})\right]\tilde{P}_{i,j}^{n+1/2}+\frac{\Delta t}{2\Delta x^2}B_{i+1,j}\tilde{P}_{i+1,j}^{n+1/2}\quad . \tag{10}$$

To this end, the advantage of the ADI method is clearly seen. Suppose at $t = n\Delta t$, P^n is known for all $x = i\Delta x$ and $y = j\Delta y$ ($n = 0$ is determined by the initial condition), so that the terms on the right-hand side of Eq. (9) are known. Eq. (9) now becomes a one-dimensional (1-D) difference equation for $\tilde{P}^{n+1/2}$ in the x-direction, which can be solved to find $\tilde{P}^{n+1/2}$ with the given boundary conditions at $x = 0$ and $x = I\Delta x$. Once $\tilde{P}^{n+1/2}$ is found, the terms on the right-hand side of Eq. (10) are known. Eq. (10) is now another 1-D difference equation for P^{n+1} in the y-direction and can be solved with the given boundary conditions at $y = 0$ and $y = J\Delta y$. In this way, the unknown function at $(n + 1)$ step P^{n+1} is found. This procedure can be repeated iteratively to find the solution at any given time $t = n\Delta t$. It can be shown that the Peaceman-Rachford ADI algorithm is unconditionally stable and has a second-order accuracy in both time and space. Furthermore, an algorithm that has the second-order accuracy in time and fourth-order accuracy in space can be constructed at the same computation cost. This algorithm is called the Mitchell-Fairweather algorithm (Ferziger, 1981). Since the matrix expressions of Eqs. (9) and (10) have triangular form, they can be efficiently solved using the Thomas algorithm (Ferziger, 1981).

APPLICATION TO THE MODELING OF LABORATORY PRESSURE TRANSIENT MEASUREMENTS

The pulse decay method for measuring the permeability of cores has been the primary application of pressure transient testing to laboratory systems. The pulse decay experiment is shown in Figure 1. Before zero time $t = 0$, the pressures of the upper and lower reservoirs P_u and P_d are equal. At $t = 0$, a pressure difference ΔP is applied at the upper reservoir by adjusting the valve of the upper reservoir. Then the up-stream pressure, P_u, will decrease and the down-stream pressure, P_d, will increase with time and they will approach a common value at a later time. The decay characteristics of P_u depend on the permeability (and permeability heterogeneity), the dimensions of the sample, and the compressive fluid storage of the upper and lower reservoirs, as well as on the compressive storage of the sample. In this study we investigate the effects of the permeability heterogeneities of the sample on the pulse decay characteristics.

We use a 2-D distribution to describe the permeability heterogeneity. In conventional laboratory measurements, rock samples are shaped into right cylinders with a circular or square cross-section. In the 2-D distribution, the permeability is assumed to vary in

$x-y$ plane (y is the axial direction) and invariant in the z direction in a square cylinder. For a circular cylinder, the 2-D heterogeneous distribution may describe the variation along and perpendicular to the axial direction. Since the effects of heterogeneities are to cause the flow behavior to deviate from that of the one-dimensional case, the use of the 2-D distribution is to capture the characteristics of the heterogeneous flow which is fundamentally a multi-dimensional phenomenon. Therefore, the results of 2-D modeling will provide physical insight to the multi-dimensional phenomenon.

The governing equation is still Eq. (1). We choose to non-dimensionize this equation by using

$$\begin{aligned} x &= L_x x' \qquad 0 \le x' \le 1 \\ y &= L_y y' \qquad 0 \le y' \le 1 \\ k &= k_0 k'(x', y') \qquad 0 \le k' \le 1. \end{aligned}$$

Then Eq. (1) becomes:

$$\frac{\partial P}{\partial t'} = \frac{\partial}{\partial x'}\left[k'(x', y')\frac{\partial P}{\partial x'}\right] + \frac{\partial}{\partial y'}\left[k'(x', y')\frac{\partial P}{\partial y'}\right] \quad , \tag{11}$$

where the dimensionless time t' is

$$t = Tt' \tag{12}$$

with the characteristic time T given by

$$T = \frac{L^2 \phi \mu}{k_0 \kappa_f} \quad . \tag{13}$$

(Here we assume $L_x = L_y = L$.) The initial condition is that at $t = 0$,

$$\begin{aligned} P|_{t=0}(x, y) &= 0 \\ P|_{t=0}(0, y) &= \Delta P \end{aligned} \tag{14}$$

or using the dimensionless quantities,

$$\begin{aligned} P'|_{t'=0}(x', y') &= 0 \\ P'|_{t'=0}(0, y') &= 1 \quad . \end{aligned} \tag{15}$$

(Without losing generality, we set the initial upper and down stream reservoir pressures to zero.) The boundary conditions are that the decrease (increase) of fluid volume in the upper (lower) reservoir per unit time equals the fluid flux flowing into (out of) the upper (lower) core boundary:

$$C_u V_u \frac{\partial P}{\partial t} = \int_A \frac{k}{\mu}\frac{\partial P}{\partial x} dA \quad x = 0 \tag{16}$$

$$C_d V_d \frac{\partial P}{\partial t} = -\int_A \frac{k}{\mu}\frac{\partial P}{\partial x} dA \qquad x = L \tag{17}$$

where $C_u V_u$ ($C_d V_d$) is the compressive fluid storage of the upper (lower) reservoir. For example, if the reservoir is a steel container filled with fluid, then C_u is the fluid compressibility $1/\kappa_f$ and V_u is the volume of the container. A is the cross area of the sample (for the 2-D problem, $dA = dy * L_z$, where L_z = unit length along the z-direction). We use the dimensionless quantities (Kamath et al., 1990)

$$\begin{cases} \beta = \dfrac{AL\phi\kappa_f}{C_u V_u} \\ \beta^* = \dfrac{AL\phi\kappa_f}{C_d V_d} \end{cases} \tag{18}$$

to denote the ratio of fluid storage of the sample to that of the upper (β) and lower (β^*) reservoirs. Using Eqs. (16), (17), and (18), the dimensionless boundary conditions are written as

$$\frac{\partial P'}{\partial t'} = \beta \int_0^1 k'(0,y')\frac{\partial P'}{\partial x'} dy' , \qquad x' = 0 \tag{19}$$

$$\frac{\partial P'}{\partial t'} = \beta^* \int_0^1 k'(1,y')\frac{\partial P}{\partial x'} dy' , \qquad x' = 1 . \tag{20}$$

As described previously, the governing equation (Eq. 1) can be solved using the ADI method, if the boundary conditions are appropriately specified. We prescribe the no-flow boundaries at $y' = 0$ and $y' = 1$, i.e.,

$$\frac{\partial P'}{\partial y'} = 0 \qquad \begin{cases} y' = 0 \\ y' = 1 \end{cases} \tag{21}$$

For the boundary conditions at $x' = 0$ and $x' = 1$, we discretize Eqs. (19) and (20) using

$$\begin{aligned} \frac{\partial P'}{\partial t'} &= \frac{P'^{n+1}(0,y') - P'^{n}(0,y')}{\Delta t'} \\ \frac{\partial P'}{\partial x'} &= \frac{P'^{n}(\Delta x',y') - P'^{n}(0,y')}{\Delta x'} . \end{aligned}$$

Then we have

$$P'^{n+1}(0,y') = \frac{\Delta t'}{\Delta x'}\beta \sum_j k'(0,j)[P'^{n}(1,j) - P'^{n}(0,j)] + P'^{n}(0,j) \qquad x = 0 \tag{22}$$

$$P'^{n+1}(L,y') = \frac{\Delta t'}{\Delta x'}\beta^* \sum_j k'(L,j)[P'^{n}(L,j) - P'^{n}(L-\Delta x',j)] + P'^{n}(L,j) \qquad x = L . \tag{23}$$

If the pressure P' at time step n is known, then Eqs. (22) and (23) represent the first kind boundary condition for P' at time step $n+1$. For the ADI method, the

boundary conditions (Eqs. 21, 22, and 23) can be readily implemented (Ferziger, 1981). In addition, for the boundary condition at $n = 0$, the initial condition Eq. (15) is also used. Solving Eqs. (9) and (10) with the given initial (Eq. 15) and boundary (Eqs. 21, 22, and 23) conditions, the pressure decay characteristics can be investigated for any permeability distributions across the sample.

NUMERICAL MODELING EXAMPLES

In this section, we present numerical modeling results for various distributions of permeability heterogeneities. The heterogeneous distributions are generated using the method described in Zhao and Toksöz (1991). Specifically, the heterogeneities are characterized by the correlation length a with respect to the model length L and different degrees of roughness of the distributions are described by using Gaussian, exponential, and Von-Karman correlation functions (Frankel and Clayton, 1986; Charrette, 1991; Zhao and Toksöz, 1991), respectively. Moreover, the anisotropic distribution of the heterogeneities can be modeled by using the ellipsoidal-shaped correlation function, which has two correlation lengths, a_1 and a_2, where a_1 is used to characterize the distribution along the semi-major axial direction, while a_2 ($< a_1$) is used along the semi-minor direction. When $a_1 >> a_2$, the heterogeneities show the lineated distribution (Zhao and Toksöz, 1991).

Analytical Solution for a Homogeneous Core Sample

In laboratory measurements of the core samples, the permeability of the sample is regarded as constant. The following 1-D analytical solution is employed to derive core permeability from the pulse decay measurements (Kamath et al., 1990):

$$P'(x',t') = \frac{1}{1+\beta+\gamma} + 2\sum_{m=1}^{\infty} \frac{\exp(-t'\phi_m^2)[\cos\phi_m x' - (\frac{\gamma\phi_m}{\beta})\sin\phi_m x']}{(1+\beta+\gamma-\gamma\phi_m^2/\beta)\cos\phi_m - \phi_m(1+\gamma+2\gamma/\beta)\sin\phi_m} \tag{24}$$

where ϕ_m are the roots of $\tan\phi = \dfrac{(\gamma+1)\phi}{\gamma\phi^2/\beta - \beta}$, and $\gamma = \dfrac{C_d V_d}{C_u V_u}$ is the ratio of the fluid storage of the upper reservoir to that of the lower reservoir.

In practice, the early time and late time portions of the pressure decay curves are used. The early time portion corresponds to the time interval where the down stream boundary has not been felt and the core appears infinite. The early time solution can be shown to obey the following differential equation (Kamath el al., 1990):

$$\sqrt{t'}\frac{dP'}{dt'} = \beta^2 P'\sqrt{t'} - \frac{\beta}{\sqrt{\pi}} \ . \tag{25}$$

Therefore, the group $(\sqrt{t'}\frac{dP'}{dt'})$ is a linear function of the group $(P'\sqrt{t'})$, with a slope β^2 and intercept $-\frac{\beta}{\sqrt{\pi}}$. Returning to the real time domain using $t' = t/T$, we have

$$\begin{cases} \text{slope} = \dfrac{\beta^2}{T} = \dfrac{k_0\beta^2}{\mu\phi C_f L^2} \\ \text{intercept} = -\dfrac{\beta}{\sqrt{\pi T}} = -\beta\sqrt{\dfrac{k_0}{\pi\mu\phi C_f L^2}} \end{cases} . \tag{26}$$

Thus, knowing the upper reservoir storage (β) and μ, ϕ, C_f, and L, Eq. (25) can be used to determine the core permeability k_0.

At the late time, the terms in the series in Eq. (24) decay to zero, and only the first term is important. It is readily shown that the late time solution obeys

$$\frac{dP'}{dt'} = -\phi_1^2\left(P' - \frac{1}{1+\beta+\gamma}\right) \tag{27}$$

or

$$\ln\left(P' - \frac{1}{1+\beta+\gamma}\right) = -\phi_1^2 t' + \text{constant} . \tag{28}$$

This shows that the pressure at the upper reservoir decays exponentially with time. If $(P' - \frac{1}{1+\beta+\gamma})$ is plotted against t', the slope of the line is $-\phi_1^2$, where ϕ_1 is the first root of

$$\tan\phi = \frac{(1+\gamma)\phi}{\frac{\gamma\phi^2}{\beta} - \beta} . \tag{29}$$

Back to real time using $t' = t/T$, we see that

$$\text{slope (late time)} = -\phi_1^2\frac{k_0}{\mu\phi C_f L^2} . \tag{30}$$

Thus the core permeability can also be determined from the slope of the late time curves. In fact, this is the theoretical background for the pulse decay method used by Brace et al. (1968).

When the core permeability is heterogeneous across the sample, the 1-D analytic solutions [(Eqs. (26), and (27)) are still used to determine core permeability, despite the permeability variation across the sample. The permeability so determined is the effective permeability of the heterogeneous sample. Our primary interest here is to investigate how the heterogeneities affect the measured effective permeability.

Gaussian Versus Homogeneous Distributions

Two groups of calculations were carried out. The first group is a heterogeneous Gaussian distribution (with correlation length $a = 5$, model length = 64), as shown in Figure 2a. The second group is a homogeneous distribution, whose permeability is the average value of the Gaussian distribution over the 2-D grids, i.e., $k' = 0.5$, if $k'(x', y')$ $(0 < k' < 1)$ is given by the Gaussian distribution. The calculations were performed for $\beta = 0.001$, 0.1, 1, and 10 ($\gamma = 1$). The results are compared in Figure 3. The pulse decay curves ($P' \sim \log_{10} t'$) for the constant distributions fit almost exactly with the 1-D analytical solutions for the various β values (see also Kamath et al., 1990). The results for the Gaussian distribution (dashed curves) differ from the constant permeability only for larger β values ($\beta = 1$, and 10). This result is in agreement with the result of Kamath et al. (1990). That is, when the core fluid compressive storage is very small compared to the storage of the reservoir, a heterogeneous and a homogeneous core with the same (average) permeability are effectively the same.

We now compare the early time result from the Gaussian and from the homogeneous distributions. Using Eq. (25), the results for $\beta = 0.1$, 1, and 10 are plotted in Figures 4a, b, and c. It can be seen that the slopes of the curves determined by Eq. (25) are different for the two distributions. The slopes for the Gaussian distribution are always greater than those of the constant distribution. If we treat the Gaussian case as a constant distribution with an effective permeability using Eq. (25), the permeability for the Gaussian case appears to be greater than its average permeability. However, with increasing β values, the difference becomes smaller. For $\beta = 10$, the slopes of the two cases are quite close (Figure 4c).

The late time solutions of the curves in Figure 3 are plotted in Figure 5 using Eq. (28). It is seen that the Gaussian and homogeneous solutions have similar slopes for the linear part of the $\ln(P' - \frac{1}{1+\beta+\gamma}) \sim t'$ relationship. This means that the effective permeability measured using the late time solution will be approximately the same for the two distributions if we apply the analytical solution (Eq. 28) to the linear portion of the curves to derive the permeability.

To explain the physical process involved in the early time and late time solutions, we plot the pressure fields for $t' = 0.1$ (early time, Figure 6a) and $t' = 3$ (late time, Figure 6b) ($\beta = 1$). For the early solution, the front of the pressure pulse (i.e., the zero pressure contour) has not reached the down stream boundary. Thus the decay is largely controlled by the permeability distribution near the upper boundary, whereas in the late time, the fluid pressure has completely penetrated the core sample and the pressure pulse decay is controlled by permeability distribution across the whole sample. In this case, the decay is not sensitive to the details of the distribution, but is controlled by the average (i.e., effective) permeability over the entire sample. Therefore, the late

time solution offers a method for measuring the effective permeability of the core sample along the direction of measurement, while the early time solution can be used to detect the heterogeneity of the sample (Kamath et al., 1990).

Gaussian Versus Fractal Distributions

To investigate the effects of fine structures of the heterogeneous distribution on transient flow, we generate a fractal distribution (Figure 2b) using the von-Karman correlation function (Frankel and Clayton, 1986), with the same correlation length as the Gaussian case in Figure 2a. Compared with Figure 2a, the fractal distribution shows fine structures and is much rougher than the Gaussian heterogeneities. The up and down stream pressure response curves calculated for the two distributions are shown in Figure 7 for $\beta = 1$ and $\beta = 10$. Despite the roughness of the fractal distribution, the pressure curves for the fractal case (dashed curves) are almost identical to those for the Gaussian case (solid curves), showing that the pressure transient is insensitive to the details of the heterogeneous distribution. This is also the case for steady fluid flow as studied by Zhao and Toksöz (1991).

Aligned Distributions

Using the method of Zhao and Toksöz (1991), we can generate aligned distributions for the heterogeneities. For the steady flow core, the permeability of the core sample as a function of the direction ($0^o < \theta < 90^o$) of the alignment was modeled by Zhao and Toksöz (1991). For the present transient flow case, we model the measurement of permeability using the same distribution. For the aligned distribution, the correlation length in the semi-major axial and semi–minor axial directions are $a_1 = 20$ and $a_2 = 2$, respectively. The pressure decay curves are calculated for various θ values varying from 0^o to 90^o. As an example, the aligned medium at $\theta = 45^o$ is shown in Figure 8. The decay curves calculated for $\beta = 1$ are shown in Figure 9. By measuring the slope of the late time solution using Eq. (28), the permeability as a function of θ can be determined. The permeability is the maximum along $\theta = 0^o$ and becomes minimum along $\theta = 90^o$. The permeability anisotropy [defined as $(k_0 - k_{90})/(k_0 + k_{90})/2$] for this case is about 10%. The degree of anisotropy for the transient flow case is similar to that of the steady flow case studied by Zhao and Toksöz (1991). The reason for this small anisotropy is that, in the aligned heterogeneous Gaussian model, a region with moderate and low permeabilities is sandwiched between two adjacent high permeability regions. But the permeability contrast between the high permeability region and the background is not very large. As a result, the flow (steady or transient) can always cross the less permeable region without having to flow around the region. Therefore, as in the steady flow case, due to the presence of background permeability, the lineation of random heterogeneities

cannot result in an anisotropic permeability that is an order of magnitude difference. In order to produce a strong permeability anisotropy, the permeability contrast between the background and the high permeability regions must be very large. This will be the case of fractures studied in the following section.

Aligned Fracture Model

Since fractures can contribute significantly to reservoir permeability, it is important to model the effects of fracture permeability. A primary effect of fracture is anisotropy in permeability in the presence of aligned fractures (Gibson and Toksöz, 1990; Zhao and Toksöz, 1991). The major features of the fracture fluid flow (steady or transient) are that the background has very small permeability, and that the flow is highly channeled along the fractures. The aligned fracture can be modeled by using the previous aligned heterogeneous distribution as follows: we choose the aspect ratio, $a_1/a_2 \gg 1$, so that the heterogeneities are highly lineated. To remove the background permeability, we set a threshold, say, 60% of the maximum $k'(x, y)$. The values of $k'(x, y)$ that are smaller than this threshold are set to a very small number (about 1/600 that of the maximum value). Although the background permeability may still be large compared to typical fracture rocks (granite, limestone, etc.), the highly conductive channels (fractures) conduct most of the flow so that the background flow is very small. In this way, transient flow in the fracture network is simulated.

Figure 10 shows the heterogeneous permeability distribution for the aligned fracture case, in which $a_1 = 20$, $a_2 = 2$, and model length = 128. Rotating this distribution from 0^o to 90^o, we calculated the transient pressure decay curves for various θ values. Figure 11 shows the decay curves for $\theta = 0^o$, $\theta = 45^o$, and $\theta = 90^o$ ($\beta = 1$). As we can see from this figure, from 0^o to 90^o, the pressure decay curve has increasingly higher values at certain time t', showing a decreasing decay rate with increasing θ values. This indicates that the pressure transient shows smaller effective permeability across the model as θ increases. In this case, the measured effective permeability can differ significantly from the permeability average over the 2-D grids, depending on the θ values. The explanation of this permeability anisotropy is similar to the steady flow case modeled by Zhao and Toksöz (1991). That is, in the aligned fracture case, flow takes a longer path to reach the down stream boundary when $\theta > 0$ than when $\theta = 0$. Because the late time solution offers a way to measure the effective permeability of the model along the x-direction, we use Eq. (28) to determine the effective permeability versus θ using the late time solution. The results are shown in Figure 12. In this figure, the permeability is the maximum along fractures and the minimum perpendicular to them. The permeability anisotropy is about 180%. This order of permeability anisotropy is in agreement with the steady flow case modeled by Zhao and Toksöz (1991).

CONCLUSIONS

In this study, we employed a stable finite difference algorithm for modeling transient fluid flow in heterogeneous porous media. We applied the algorithm to the modeling of laboratory pressure transient testing of core permeabilities. The early time portion of the pulse decay curve can be used to characterize the permeability heterogeneity of the core sample. The late time portion can be used to measure the effective permeability of the core sample, especially when the fluid storage of the core is small compared to that of the upper stream reservoir. The transient flow is affected by the lineation in the permeability distributions. However, if the permeability contrast between the high permeability region and the background is not large, the lineation of the permeability distribution does not result in anisotropy of an order of magnitude. Nevertheless, in cases of aligned fractures where the background permeability is small, significant anisotropy in permeability measured using the transient method does exist, as in the case of steady fluid flow.

In the field test of permeability using pressure transients in a borehole, it is important to understand the effects of the in-situ heterogeneities on the measured permeability. The numerical analysis of this problem can be carried out by developing the finite difference algorithm for the cylindrical coordinates system. This will be the topic of future research.

ACKNOWLEDGEMENT

This research was supported by the Borehole Acoustics and Logging Consortium at M.I.T., and Department of Energy grant DE-FG02-86ER13636.

REFERENCES

Bernabé, Y., 1991, On the measurement of permeability in anisotropic rocks. In press in *Fault Mechanism and Transport Properties of Rocks: A Festchrift in Honor of W.F. Brace* edited by B. Evans and T.F. Wong, Academic Press, London.

Brace, W.F., J.B. Walsh, and W.T. Frangos, 1968, Permeability of granite under high pressure, *J. Geophys. Res., 73*, 2225–2236.

Charrette, E.E., 1991, *Elastic Wave Scattering in Laterally Inhomogeneous Media*, Ph.D. Thesis, M.I.T., Cambridge, MA.

Ferziger, J.H., 1981, *Numerical Methods for Engineering Applications*, John Wiley &

Sons, Inc., New York.

Frankel, A., and R. Clayton, 1986, Finite difference simulations of seismic scattering: implications for the propagation of short-period seismic waves in the crust and models of crustal heterogeneity, *J. Geophys. Res., 91*, 6465–6489.

Gibson, R.L. Jr., and M.N. Toksöz, 1990, Permeability estimation from velocity anisotropy in fractured rock, *J. Geophys. Res., 95*, 15643–15655.

Kamath, J., R.E. Boyer, and F.M. Nakagawa, 1990, Characterization of core scale heterogeneities using laboratory pressure transients, *Society of Petroleum Engineers*, 475–488.

Melville, J.G., F.J. Molz, O. Güven, and M.A. Widdowson, 1991, Multilevel slug tests with comparisons to tracer data, *Ground Water, 29*, 897–907.

Zhao, X.M. and M.N. Toksöz, 1991, Permeability anisotropy in heterogeneous porous media, *SEG ABSTRACTS, D/P1.7*, 387–390.

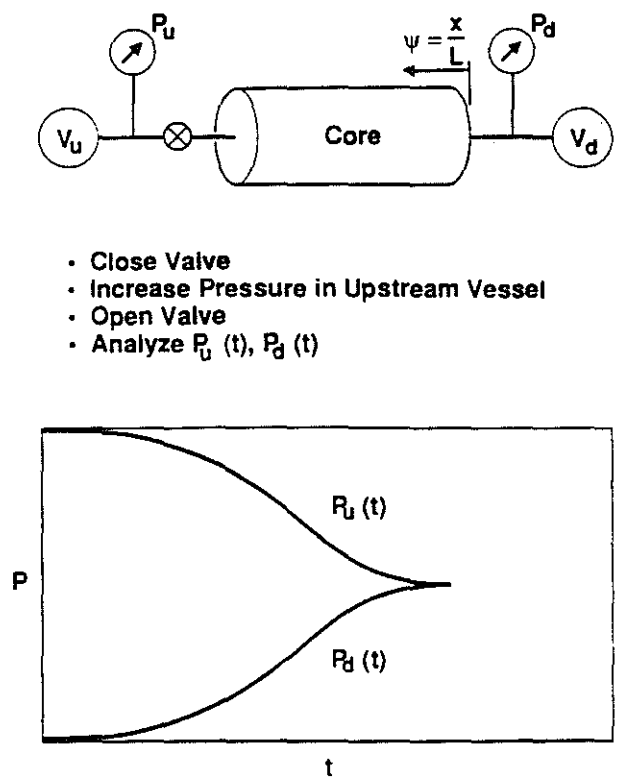

Figure 1: Pulse decay test methodology (from Kamath el al., 1990).

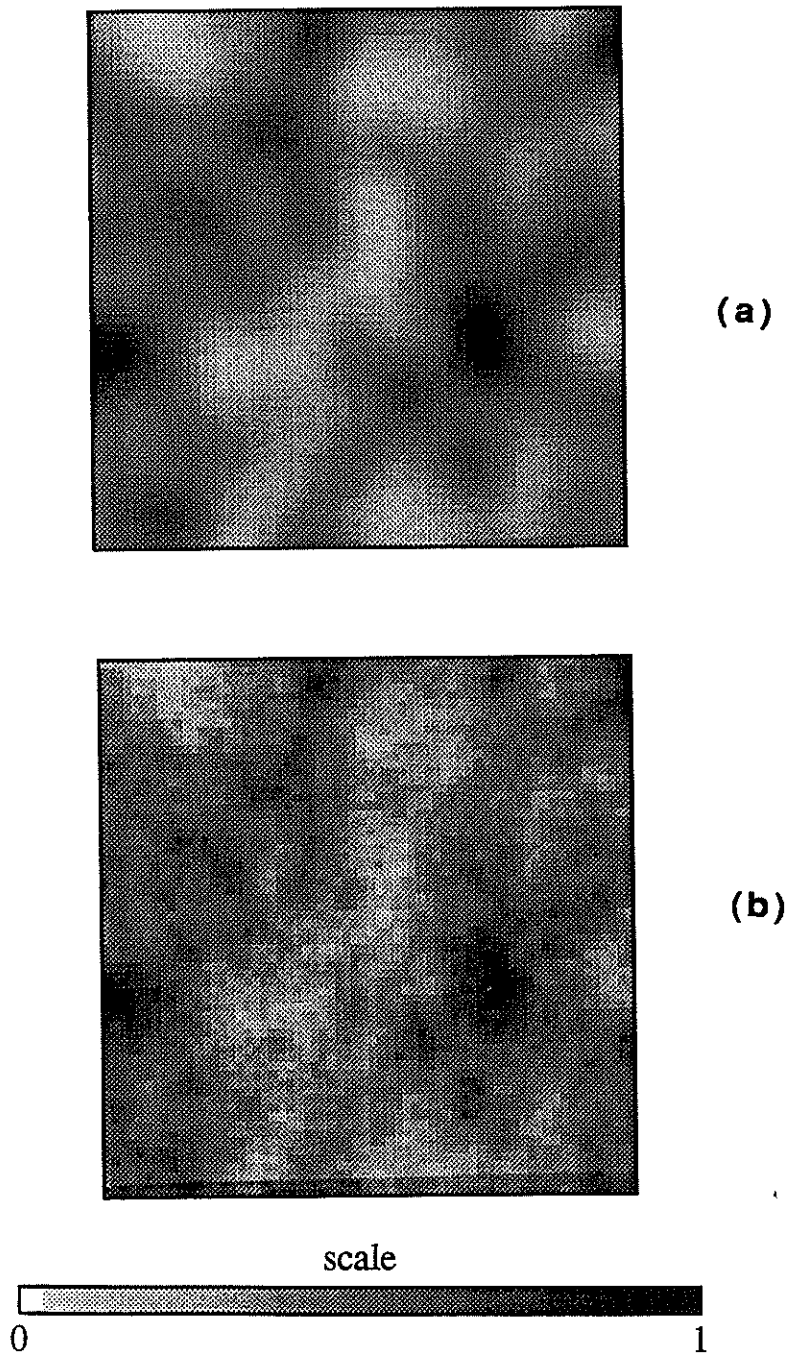

Figure 2: Heterogeneous Gaussian (a) and fractal (b) distributions with correlation length $a = 5$ and model length $L = 64$.

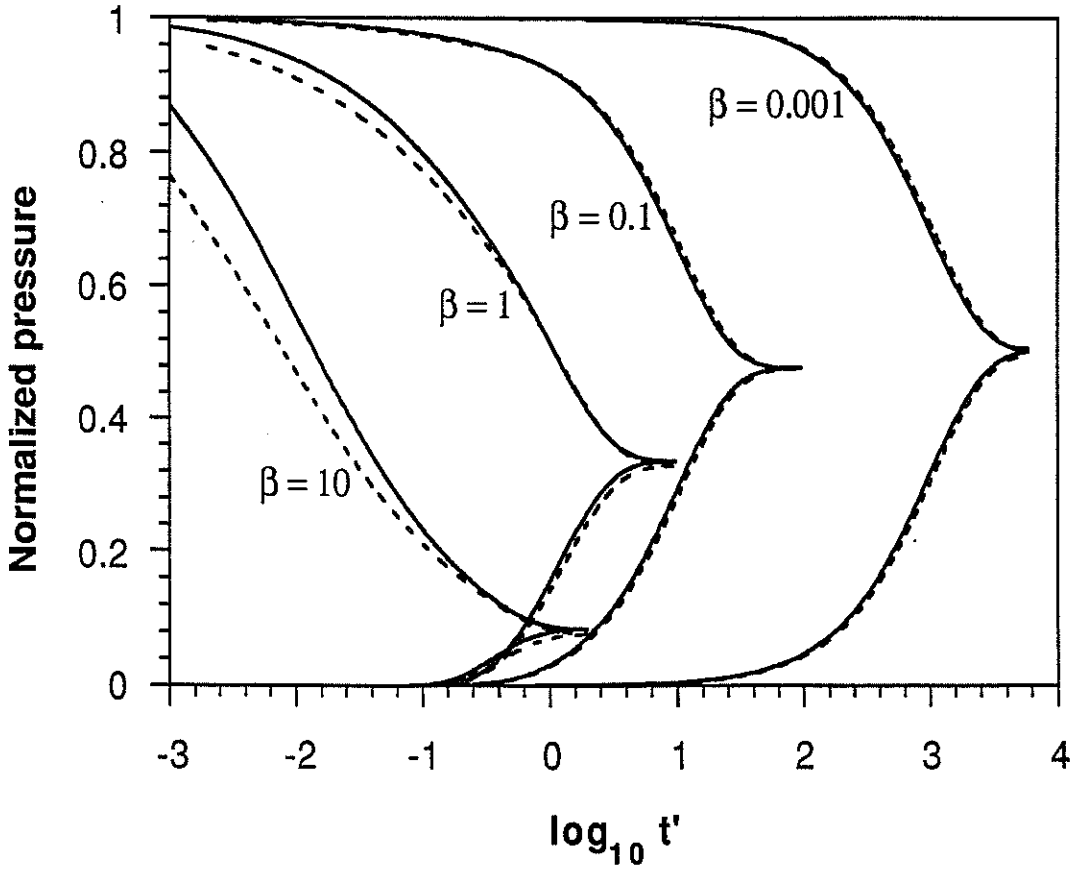

Figure 3: Pulse response curves for homogeneous (solid) and Gaussian (dashed) distributions.

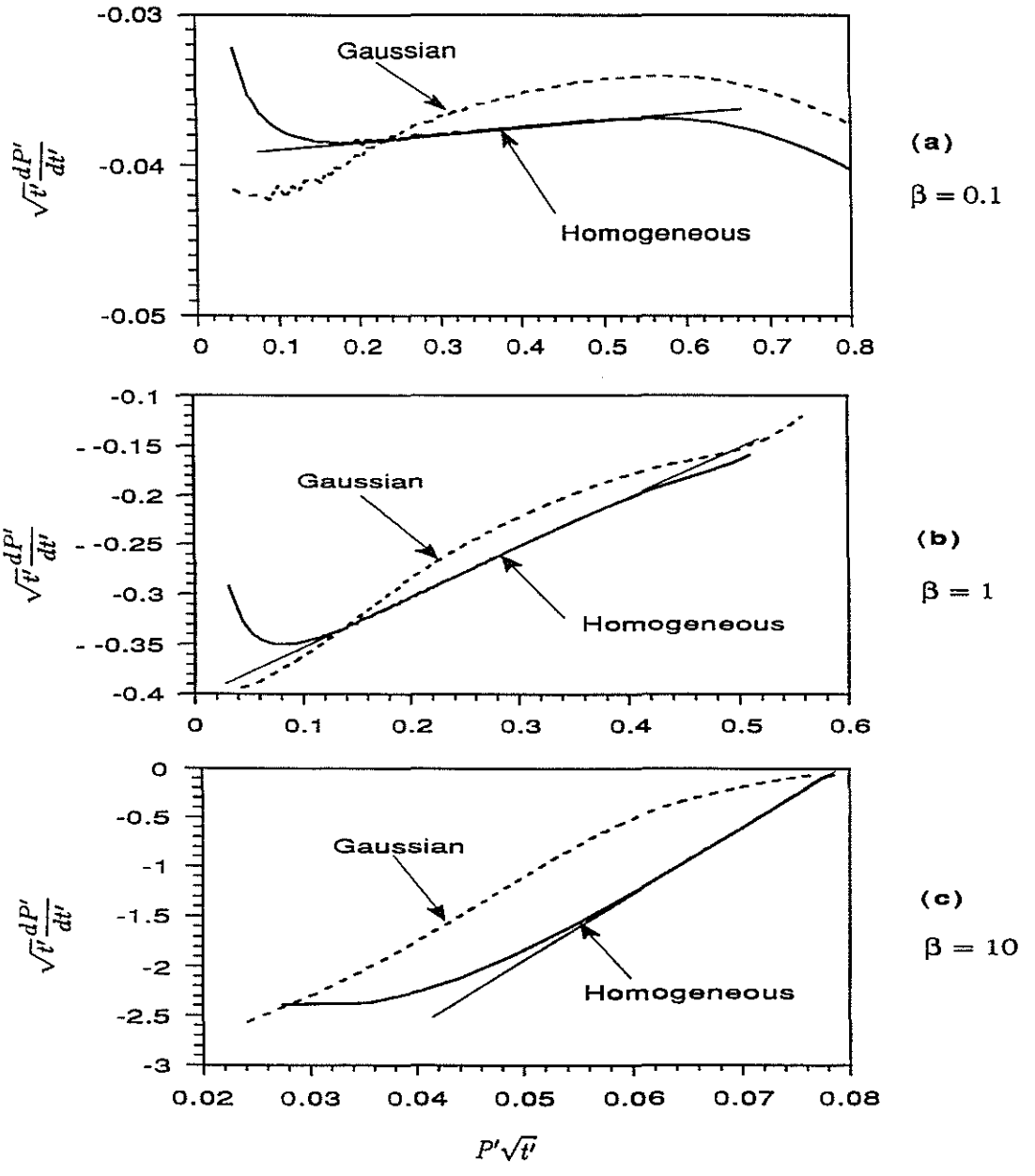

Figure 4: Comparison of early time solution for homogeneous and Gaussian distributions: (a) $\beta = 0.1$, (b) $\beta = 1$, and (c) $\beta = 10$ with increasing β, the slopes of the two solutions become similar.

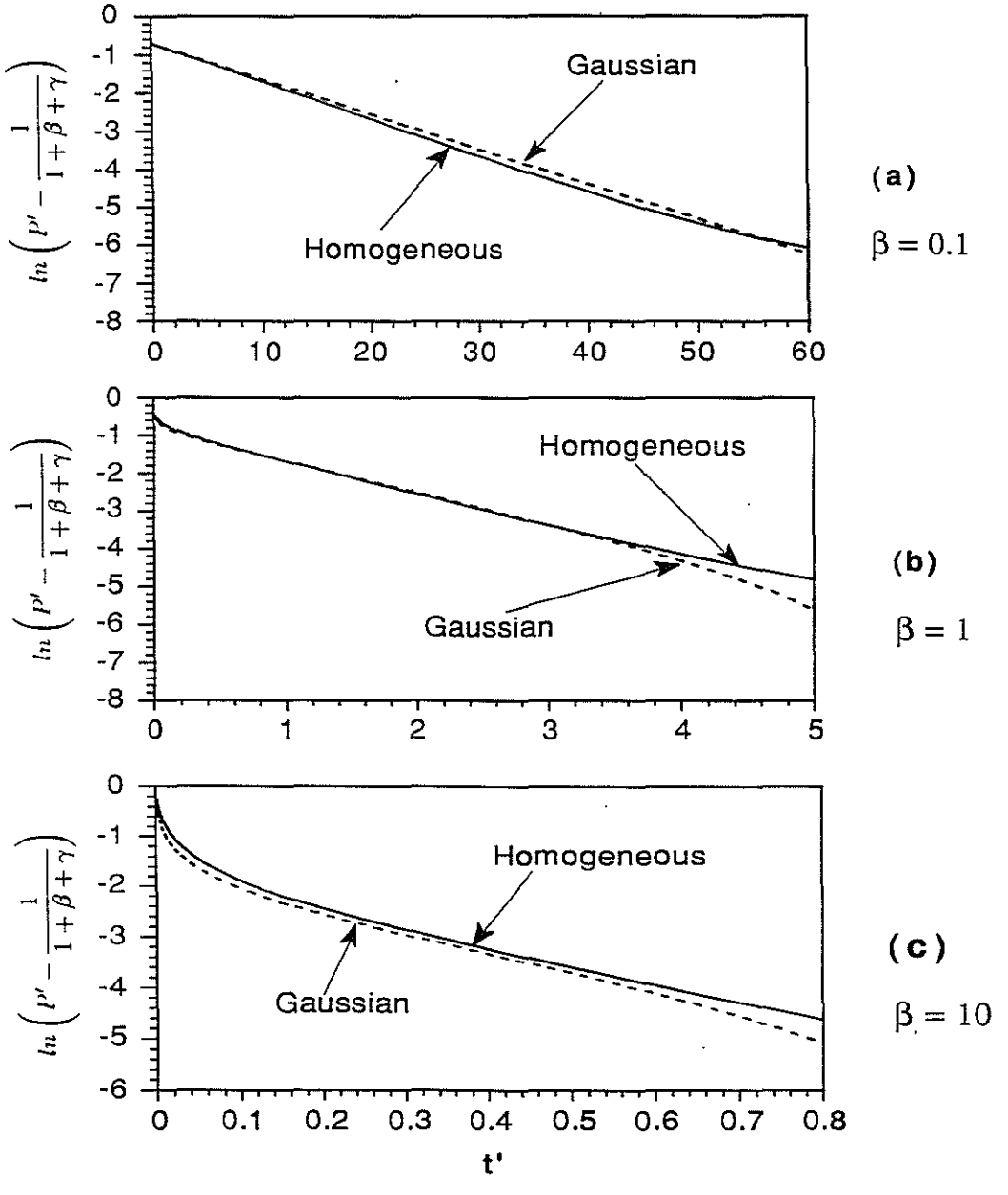

Figure 5: Comparison of late time solution for homogeneous and Gaussian distributions: (a) $\beta = 0.1$, (b) $\beta = 1$, and (c) $\beta = 10$. The slopes of the solutions are almost the same for the two distributions.

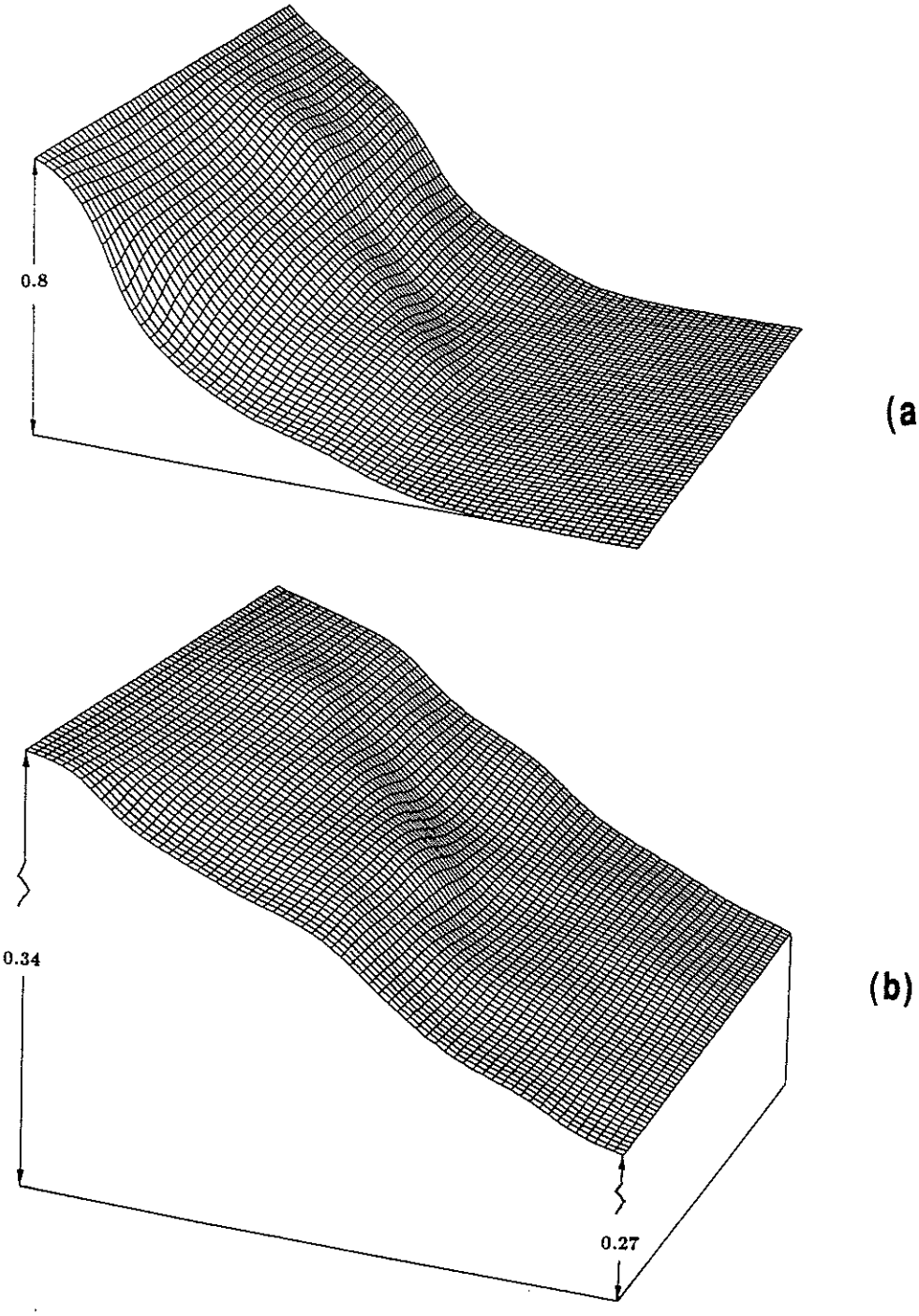

Figure 6: Pressure field at (a) early time ($t' = 0.1$) and (b) late time ($t' = 3$). For the early time, the pressure has not reached the lower boundary. For the late time, the pressure has penetrated the lower boundary and the amplitudes are reduced.

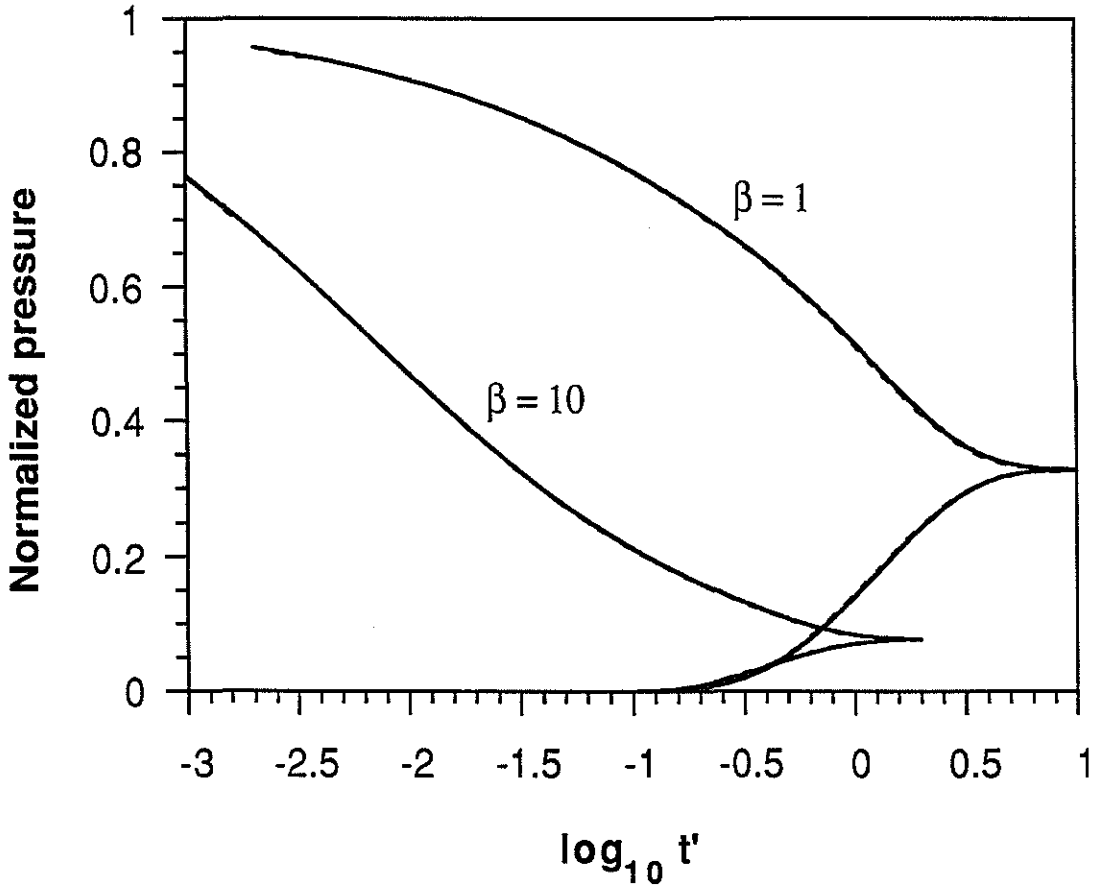

Figure 7: Comparison of pressure responses of Gaussian (solid curves) and fractal (dashed curves) heterogeneous distributions.

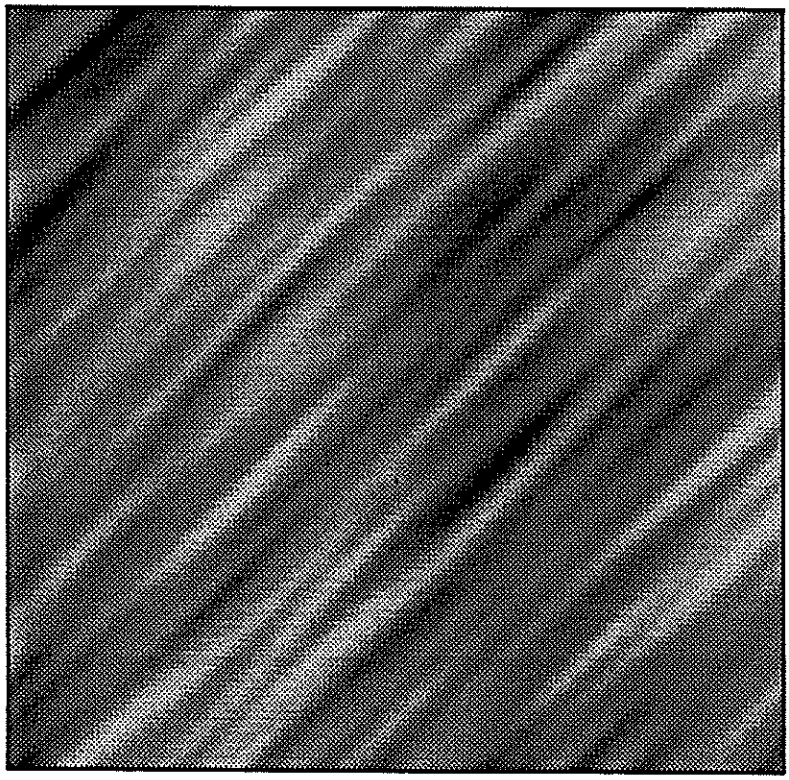

Figure 8: Example of aligned Gaussian distribution ($\theta = 45^o$), with $1 = 20$, $a_2 = 2$, and the model length is 64.

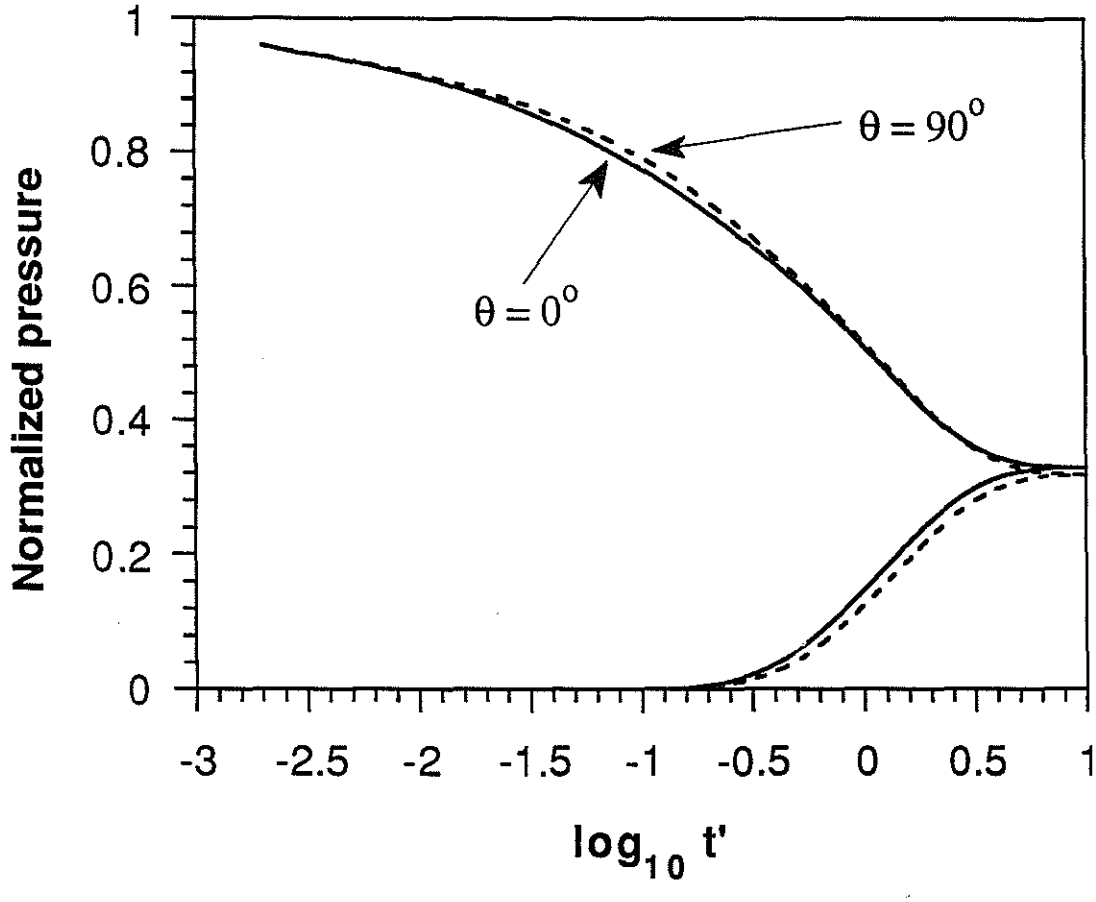

Figure 9: Pulse response curves of the aligned distributions at $\theta = 0^o$ (solid) and $\theta = 90^o$ (dashed) for $\beta = 1$.

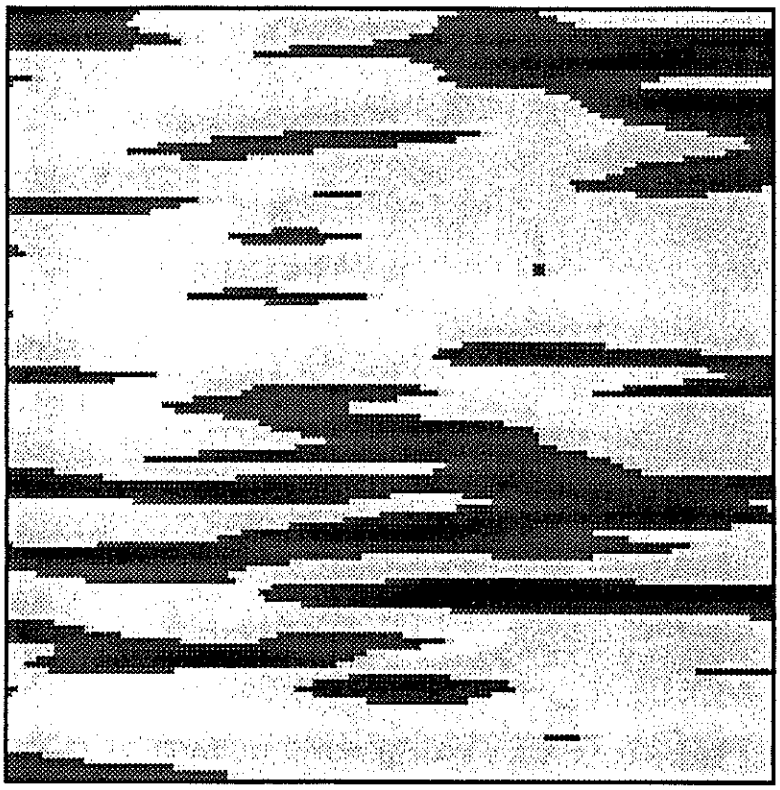

Figure 10: Example of aligned fracture model ($\theta = 0°$).

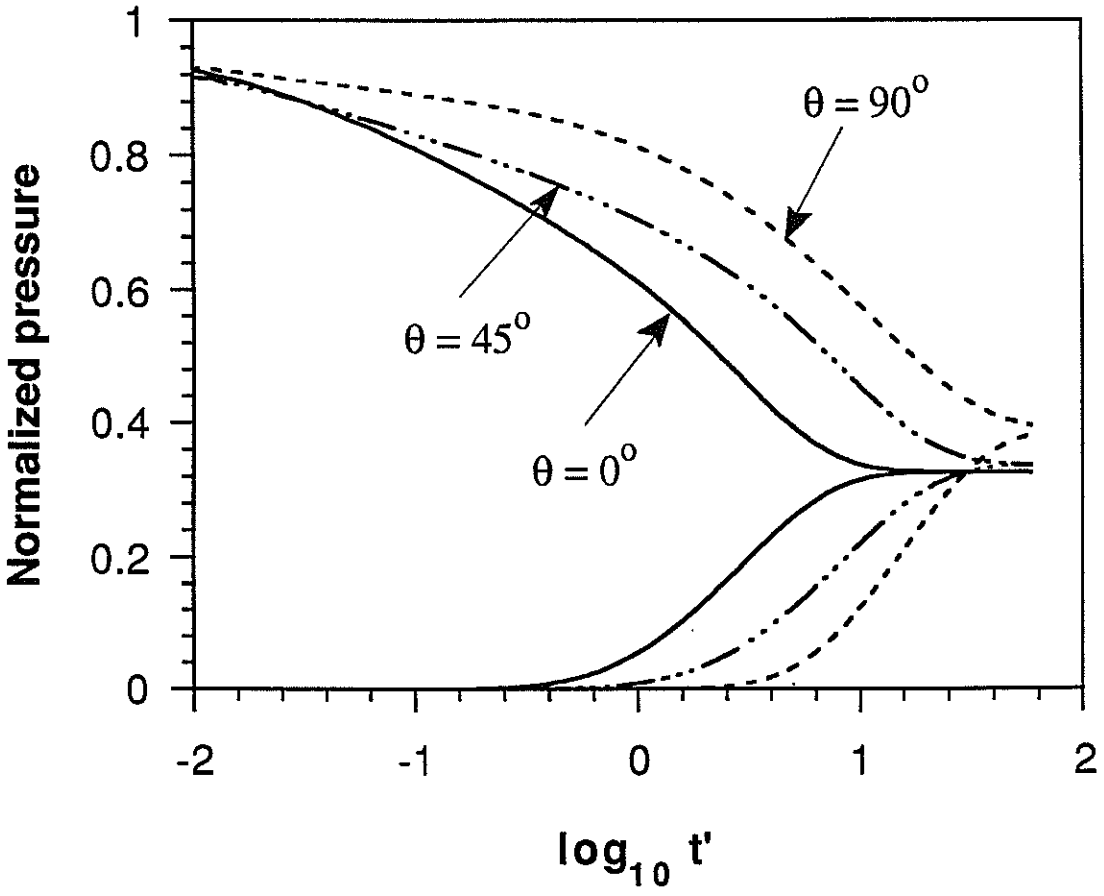

Figure 11: Pulse response curves of fractured medium at $\theta = 0^o$, 45^o, and 90^o.

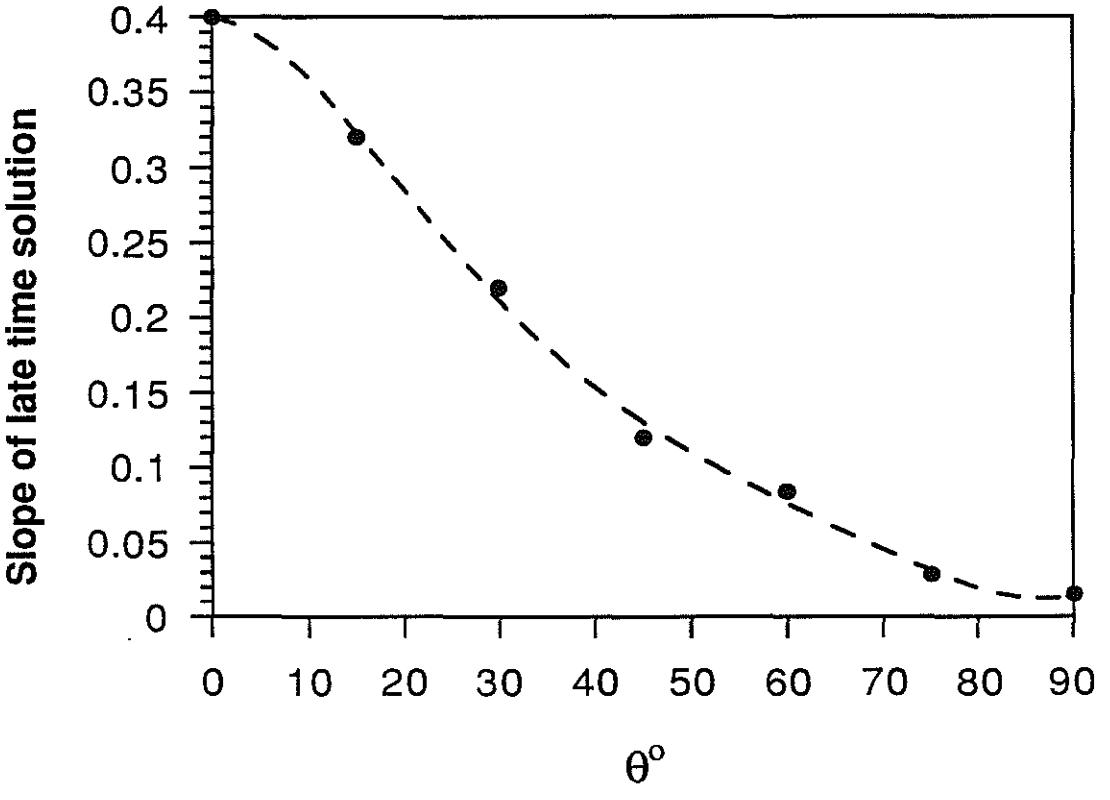

Figure 12: Normalized permeability of late time solution versus fracture alignment angle θ.